International Journal of Heat and Mass Transfer 52 (2009) 3510–3517

Contents lists available at ScienceDirect

International Journal of Heat and Mass Transfer

journal homepage: www.elsevier.com/locate/ijhmt

Comparison of thermal performances of plate-fin and pin-fin heat sinks subject to an impinging flow

Dong-Kwon Kim, Sung Jin Kim *, Jin-Kwon Bae

Department of Mechanical Engineering, Korea Advanced Institute of Science and Technology, Daejeon 305-701, Republic of Korea

ARTICLE INFO

Article history:
Received 16 September 2008
Received in revised form 26 February 2009
Accepted 26 February 2009
Available online 15 April 2009

Keywords:
Heat sink
Impinging flow
Thermal resistance

ABSTRACT

In this paper, we compare thermal performances of two types of heat sinks commonly used in the electronic equipment industry: plate-fin and pin-fin heat sinks. In particular, heat sinks subject to an impinging flow are considered. For comparison of the heat sinks, experimental investigations are performed for various flow rates and channel widths. From experimental data, we suggest a model based on the volume averaging approach for predicting the pressure drop and the thermal resistance. By using the model, thermal resistances of the optimized plate-fin and pin-fin heat sinks are compared. Finally, a contour map, which depicts the ratio of the thermal resistances of the optimized plate-fin and pin-fin heat sinks as a function of dimensionless pumping power and dimensionless length, is presented. The contour map indicates that optimized pin-fin heat sinks possess lower thermal resistances than optimized plate-fin heat sinks when dimensionless pumping power is small and the dimensionless length of heat sinks is large. On the contrary, the optimized plate-fin heat sinks have smaller thermal resistances when dimensionless pumping power is large and the dimensionless length of heat sinks is small.

1. Introduction

Recent advances in semiconductor technology have led to a significant increase in power densities encountered in microelectronic equipment [1,2]. Accordingly, effective cooling technology is essential for reliable operation of electronic components [3,4]. Various types of cooling systems have been developed as thermal solutions. In this regard, a heat sink is the most widely used type of cooling device and has received much attention due to its cost-effective performance. Two common types of heat sinks which are widely used in the industry are plate-fin heat sinks and pin-fin heat sinks. The former offers simple design and easy fabrication, while the latter has an advantage of providing higher heat transfer coefficient at the expense of higher production cost. Given that the two types of heat sinks have respective strengths, a considerable body of research has been concentrated on both configurations.

Numerous studies have focused on the plate-fin heat sink subject to an impinging flow. Biber [5] numerically studied a number of different combinations of channel parameters and presented a correlation for the average Nusselt number for a plate-fin heat sink. Kondo et al. [6] used a semi-empirical zonal approach for determining the thermal resistance as well as the pressure drop for a plate-fin heat sink. In their model, the heat sink was divided into six regions, each of which was solved separately. Duan and Muzychka [7] also developed a simple semi-empirical model for predicting the heat transfer coefficient of plate-fin heat sinks. Meanwhile, many studies have also dealt with the pin-fin heat sink subject to an impinging jet. A numerical simulation of the three-dimensional flow and temperature field was performed by Sathe et al. [8]. Ledezma et al. [9] presented a simplified numerical model to obtain correlations for the optimal fin spacing of pin-fin heat sinks. Kondo et al. [10] suggested a semi-empirical zonal model for a pin-fin heat sink. The flow behavior and heat transfer due to air jet impingement on pin-fin heat sinks was experimentally studied by Issa and Ortega [11].

As noted above, the plate-fin and pin-fin heat sinks are both commonly used and studied as cooling solutions for electronic equipment. Then, an obvious question is which type of heat sink has better performance? To date, several researchers have been interested in this question and sought proper answers. Kondo et al. used a zonal approach in optimizing the thermal performance of plate-fin and pin-fin heat sinks under the constraint of fixed pumping power and heat sink size. They showed that optimized plate-fin heat sinks provide 40% lower thermal resistances compared to optimized pin-fin heat sinks [12]. Li et al. [13] compared thermal resistances of several plate-fin and pin-fin heat sinks with various fin heights and Reynolds numbers experimentally using infrared thermography. Contrary to the results presented by Kondo et al., they concluded that the thermal performance of the pin-fin heat sink is superior to that of the plate-fin heat sink. As indicated by these contradictory results, the selection between the plate-fin and pin-fin heat sinks is still not obvious. Furthermore, previous

* Corresponding author. Tel.: +32 350 3043; fax: +32 350 8207.
E-mail address: sungjinkim@kaist.ac.kr (S.J. Kim).

0017-9310/$ - see front matter © 2009 Elsevier Ltd. All rights reserved.
doi:10.1016/j.ijheatmasstransfer.2009.02.041

Nomenclature

a	wetted area per volume
c	heat capacity of fluid
h	heat transfer coefficient based on one-dimensional bulk mean temperature
H	channel height
k	thermal conductivity
K	permeability
L	length of heat sink (=width of heat sink)
L^*	dimensionless length of heat sink (L/H)
p	pressure
P_{Pump}	pumping power
P^*_{Pump}	dimensionless pumping power ($P_{Pump}/\mu_f^3\rho_f^{-2}H^{-1}$)
q	heat transfer rate
R	total thermal resistance
T	temperature
u,v,w	velocity
U,V,W	characteristic velocity
v_0	inlet velocity
w_c	channel width
w_c^*	dimensionless channel width (w_c/H)
w_w	fin thickness
x,y,z	Cartesian coordinate system
$\langle\ \rangle$	averaged value
$\langle T\rangle^{b,f}$	one-dimensional bulk mean temperature for the fluid phase

Greek symbols

ε	porosity ($w_c/(w_c+w_w)$)
η	similarity variable
η_{eff}	fin efficiency
μ	viscosity
θ	dimensionless temperature
ρ	density
Ψ	stream function

Subscripts

bm	bulk mean
f	fluid
in	inlet
opt	optimized
pin	pin-fin heat sink
$plate$	plate-fin heat sink
s	solid
w	wall

Superscripts

f	averaged value over the fluid region
s	averaged value over the solid region

works did not compare the optimized plate-fin and pin-fin heat sinks systematically for various pumping powers and the heat sink sizes. Kondo et al. did not show the effect of the size, while Li et al. did not optimize the geometry of the heat sink.

The objectives of the present paper are to eliminate ambiguity associated with the selection of a heat sink type and to compare the thermal performance of the optimized plate-fin and pin-fin heat sinks for various pumping powers and the heat sink sizes. For this comparison, experimental investigations are performed for various flow rates and channel widths. Then, from experimental data, we suggest a model based on the volume averaging method for predicting the pressure drop and the thermal resistance. By using the model, thermal resistances of the optimized plate-fin and pin-fin heat sinks are compared. Finally, a contour map, which depicts the ratio of the thermal resistances of the optimized plate-fin and pin-fin heat sinks as a function of dimensionless pumping power and dimensionless length, is presented. This study will help engineers to choose a heat sink with better performance between the two types of heat sinks subject to an impinging jet.

2. Experiments

In this section, the experimental portion of the present study is described. Two types of fin designs, plate-fin and inline square pin-fin heat sinks, have been tested as shown in Figs. 1(a), 2(a), and 3. The dimensions of the heat sinks are shown in Table 1. The tested heat sinks are made of aluminum alloy 6061 (k = 170 W/m K) and no additional surface treatment is applied.

The general layout and a photo of the experimental apparatus are shown in Figs. 4 and 5, respectively. The gas flows into the wind tunnel from a pressure tank through a metering valve and a mass flow meter. The flow meter is used for measuring the flow rate in the wind tunnel (D08-8C, Sevenstar electronics). The wind tunnel walls are made of acrylic (k = 0.86 W/m K). In order to measure the pressure difference between the inlet and the outlet of the heat sink, a pressure tap is positioned on the wind tunnel wall and is connected to a manometer (FCO510, Furness). To measure the temperatures at the base of the fins, seven 30 gauge J-type thermocouples (Omega) are mounted through 3 mm deep holes of a base

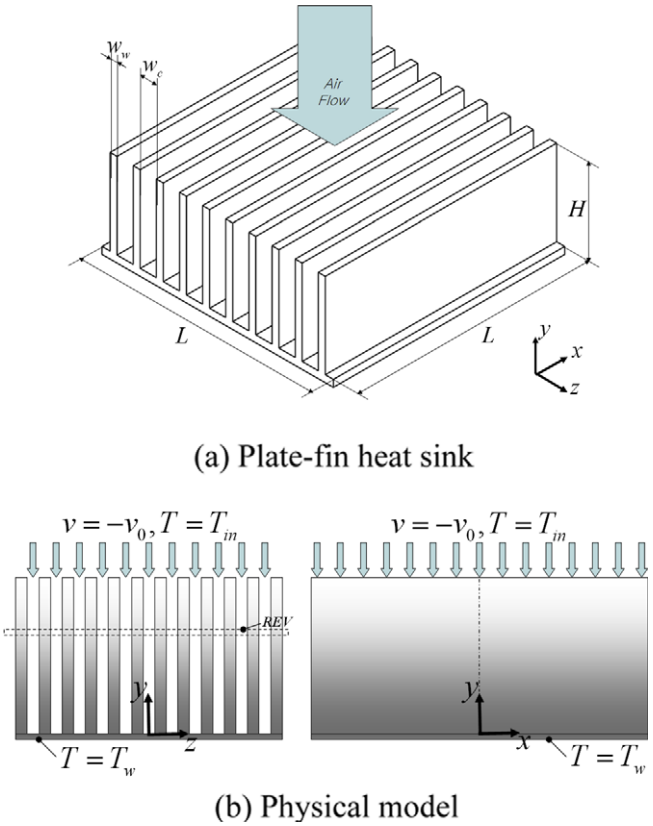

Fig. 1. Schematic diagrams for plate-fin heat sink subject to an impinging flow.

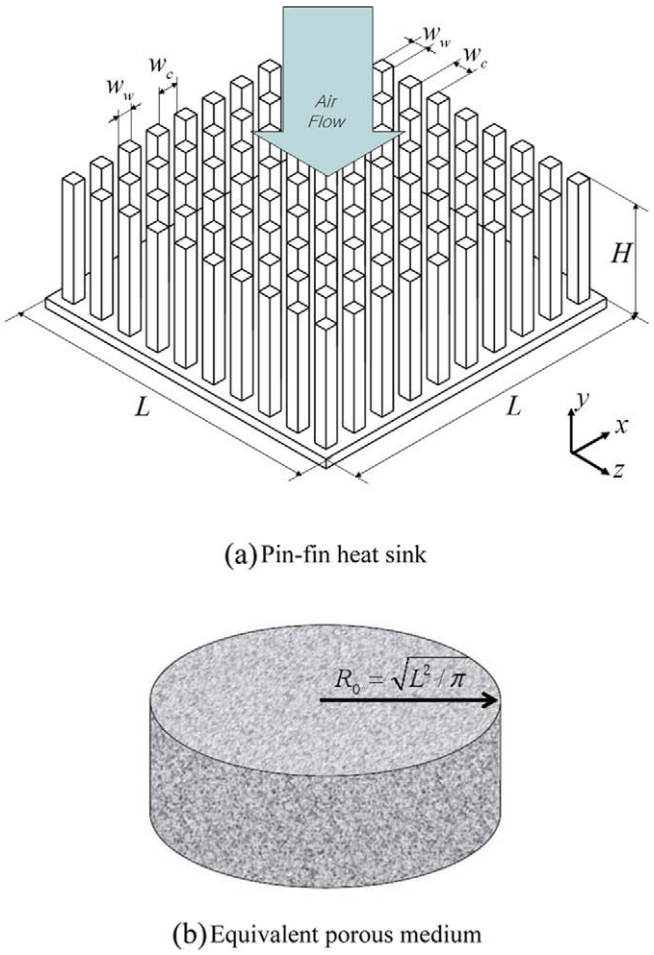

Fig. 2. Schematic diagrams for pin-fin heat sink subject to an impinging flow.

plate having 5 mm thickness. The relative positions of thermocouples for temperature measurement are shown in Fig. 4. The maximum heat sink base temperature is measured from readings of seven thermocouples. An Agilent 34970A DAQ is used to transport data measured by the thermocouples. From the analysis of the experimental uncertainties, maximum uncertainties for measurement of the pressure drop and the temperature are estimated to be 5% and 2%, respectively. The heat sinks are heated by electrical heaters fabricated using stainless steel with 0.25 mm thickness sandwiched by Kapton® films. To reduce heat loss, the bottom of the heater is insulated with Teflon. The heat loss is determined from a surface temperature measurement of the test section. To calculate the net heat flux at the bottom of the heat sink, the estimated heat loss is subtracted from the electric power supplied to the heater. The heat supplied from the power supply is calculated by measuring the voltage drop and the current through the heater. The maximum heat loss is about 5% of the supplied heat.

A typical test procedure is as follows: Flow rate is set by regulating the metering value. The heater is then powered up to a heat load of 30 W and allowed to stabilize. The temperature distribution at the base of the heat sink is measured until the change in the temperature is smaller than ±0.1 °C in a 2 min period. We conducted experiments in the laminar flow regime with flow rates of 50, 100, 150, and 200 Standard Liter per Minute (SLM). The pumping power is calculated by multiplying the measured flow rate and pressure drop. The range of the pumping power (P_{Pump}) from 0.00082 to 0.096 W is covered in the present experiment. Each experiment was conducted four times.

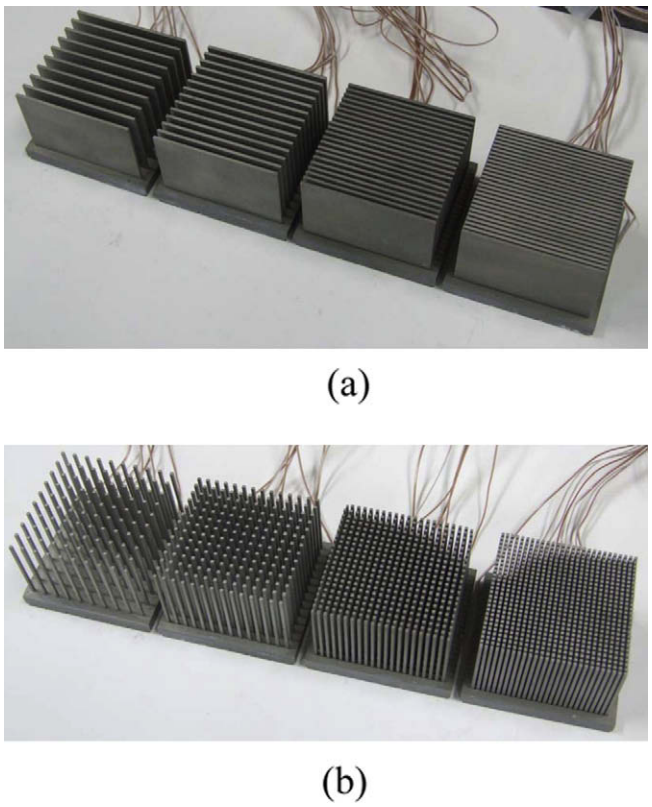

Fig. 3. Heat sinks used for experimental study: (a) plate-fin heat sink, (b) pin-fin heat sink.

Table 1
Tested heat sinks.

Type of heat sink	w_c (mm)	w_w (mm)	H (mm)	L (mm)
Plate-fin 1	0.5	1	25	40
Plate-fin 2	0.95			
Plate-fin 3	1.44			
Plate-fin 4	2			
Plate-fin 5	3.33			
Pin-fin 1	0.5	1	25	40
Pin-fin 2	0.95			
Pin-fin 3	1.44			
Pin-fin 4	2			
Pin-fin 5	3.33			

3. Mathematical modeling using the volume averaging approach

In the present study, detailed information, such as velocity and temperature distributions, is of secondary importance. Instead we are concerned with estimating the macroscopic aspects of a problem such as the pressure drop across a channel and the overall thermal resistance of a heat sink. Given that our main interest lies in the macroscopic quantities, it would be wise to average the governing equations in the direction normal to the flow. This approach can lead to considerable simplification, especially when the original problem requires a great deal of time and money for obtaining a complete solution. Since a heat transfer device is modeled as a fluid-saturated porous medium in this technique, it is frequently called a porous medium approach. This approach has been successfully applied in thermal design and optimization of heat transfer devices such as internally finned tubes and microchannel heat sinks with a parallel flow [14,15]. In this section, a modeling technique based on the volume averaging approach is proposed.

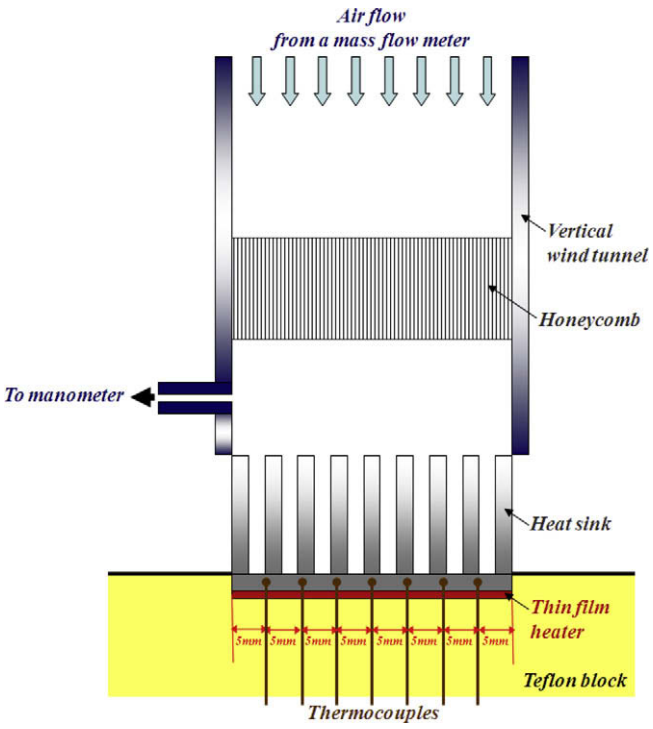

Fig. 4. Layout of the experimental apparatus.

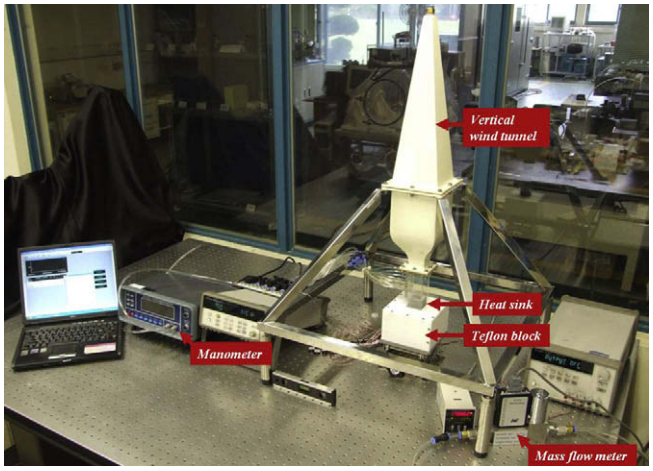

Fig. 5. Photo of the experimental apparatus.

3.1. Plate-fin heat sink

The problem under consideration is an impinging flow through a plate-fin heat sink as shown in Fig. 1(a) and (b). The bottom surface is kept constant at a high temperature. Air impinges on the heat sink along the y-axis and then flows parallel to x-axis. Air, employed as a coolant, passes through the heat sink, thus removing the heat generated by the component attached at the bottom of the heat sink substrate. In analyzing this problem, the flow is assumed to be steady and laminar. In addition, all thermal properties are evaluated at the film temperature of fluid. In addition, it is assumed that the aspect ratio of the channel is higher than 1 and the solid conductivity is higher than the fluid conductivity.

The momentum and energy equations are given as follows.

$$\rho\left(u\frac{\partial u}{\partial x}+v\frac{\partial u}{\partial y}+w\frac{\partial u}{\partial z}\right)=-\frac{\partial p}{\partial x}+\mu\left(\frac{\partial^2 u}{\partial x^2}+\frac{\partial^2 u}{\partial y^2}+\frac{\partial^2 u}{\partial z^2}\right) \tag{1}$$

$$\rho\left(u\frac{\partial v}{\partial x}+v\frac{\partial v}{\partial y}+w\frac{\partial v}{\partial z}\right)=-\frac{\partial p}{\partial y}+\mu\left(\frac{\partial^2 v}{\partial x^2}+\frac{\partial^2 v}{\partial y^2}+\frac{\partial^2 v}{\partial z^2}\right) \tag{2}$$

$$\rho c\left(u\frac{\partial T}{\partial x}+v\frac{\partial T}{\partial y}+w\frac{\partial T}{\partial z}\right)=k\left(\frac{\partial^2 T}{\partial x^2}+\frac{\partial^2 T}{\partial y^2}+\frac{\partial^2 T}{\partial z^2}\right) \tag{3}$$

In the volume averaging approach, the governing equations for the averaged velocity and temperature are established by the averaging momentum equations and energy equation. Before averaging these equations, it is necessary to define the quantities to be averaged. Since the present system has a periodic structure in the z direction, the representative elementary volume (REV) for averaging can be visualized as a rectangular parallelepiped aligned parallel to the z-axis, as shown in Fig. 1(b). The averaged quantities over the fluid and solid phases of the REV are then defined, respectively, as follows:

$$\langle\phi\rangle^f=\frac{1}{w_c}\int_0^{w_c}\phi dz,\quad \langle\phi\rangle^s=\frac{1}{w_w}\int_{w_c}^{w_c+w_w}\phi dz \tag{4}$$

For the averaged fluid temperature, the one-dimensional bulk mean temperature is more suitable than the mean temperature to calculate the thermal performance of the heat sinks. The one-dimensional bulk mean temperature is defined as

$$\langle T\rangle^{f,b}=\frac{\int_0^{w_c}Tudz}{\int_0^{w_c}udz} \tag{5}$$

As pointed out by Slattery [16], some information is lost when governing equations are averaged: in the present case, the dependence of the velocity and temperature distributions in the averaging direction is lost. For the present configuration, the lost information is recovered with an approximation. For this, it is assumed that the velocity and temperature profiles for the fluid in the averaging direction are similar to those of a Poiseuille flow between two infinite parallel plates. This assumption is similar to the assumption made for the profile shape function in obtaining integral solutions for a laminar boundary layer flow [17]. The velocity and temperature distributions for the Poiseuille flow in this configuration can be easily determined to be

$$u=6\langle u\rangle^f\cdot\frac{z}{w_c}\left(1-\frac{z}{w_c}\right) \tag{6}$$

$$T=\frac{420}{17}(\langle T\rangle^{b,f}-\langle T\rangle^s)\left(\frac{1}{6}\left(\frac{z}{w_c}\right)^4-\frac{1}{3}\left(\frac{z}{w_c}\right)^3+\frac{1}{6}\left(\frac{z}{w_c}\right)\right)+\langle T\rangle^s \tag{7}$$

The governing equations for the averaged velocity and temperature are established by averaging the momentum and energy equations with Eqs. (6) and (7).

x directional momentum equation:

$$\frac{6}{5}\rho_f\left(\langle u\rangle^f\frac{\partial\langle u\rangle^f}{\partial x}+\langle v\rangle^f\frac{\partial\langle u\rangle^f}{\partial y}\right)+\frac{\partial\langle p\rangle^f}{\partial x}=-\frac{\varepsilon\mu_f}{K}\langle u\rangle^f+\mu\left(\frac{\partial^2\langle u\rangle^f}{\partial x^2}+\frac{\partial^2\langle u\rangle^f}{\partial y^2}\right) \tag{8}$$

y directional momentum equation:

$$\frac{6}{5}\rho_f\left(\langle u\rangle^f\frac{\partial\langle v\rangle^f}{\partial x}+\langle v\rangle^f\frac{\partial\langle v\rangle^f}{\partial y}\right)+\frac{\partial\langle p\rangle^f}{\partial y}=-\frac{\varepsilon\mu}{K}\langle v\rangle^f+\mu\left(\frac{\partial^2\langle v\rangle^f}{\partial x^2}+\frac{\partial^2\langle v\rangle^f}{\partial y^2}\right) \tag{9}$$

Energy equation for the fluid phase:

$$\varepsilon\rho_f c_f\left(\langle u\rangle^f\frac{\partial\langle T\rangle^{b,f}}{\partial x}+\langle v\rangle^f\frac{\partial\langle T\rangle^{b,f}}{\partial y}\right)=ha(\langle T\rangle^s-\langle T\rangle^{b,f})+\varepsilon k_f\left(\frac{\partial\langle T\rangle^{b,f}}{\partial x^2}+\frac{\partial\langle T\rangle^{b,f}}{\partial y^2}\right) \tag{10}$$

Energy equation for the solid phase:

$$(1-\varepsilon)k_s\left(\frac{\partial\langle T\rangle^s}{\partial x^2}+\frac{\partial\langle T\rangle^s}{\partial y^2}\right)+ha(\langle T\rangle^{b,f}-\langle T\rangle^s)=0 \tag{11}$$

where ε, K, h, and a are the porosity, permeability, heat transfer coefficient, and wetted area per volume, respectively.

$$\varepsilon=\frac{w_c}{w_w+w_c} \tag{12}$$

$$a=\frac{2}{w_w+w_c} \tag{13}$$

$$K=-\varepsilon w_c\langle u\rangle^f\left(\left.\frac{\partial u}{\partial z}\right|_{z=w_c}-\left.\frac{\partial u}{\partial z}\right|_{z=0}\right)^{-1}=\frac{\varepsilon w_c^2}{12} \tag{14}$$

$$h=\frac{k_f}{2}\left(\left.\frac{\partial T}{\partial z}\right|_{z=w_c}-\left.\frac{\partial T}{\partial z}\right|_{z=0}\right)\cdot(\langle T\rangle^s-\langle T\rangle^{b,f})^{-1}=\frac{70k_f}{17w_c} \tag{15}$$

Boundary conditions are given as

$$\langle u\rangle^f=\langle v\rangle^f=0,\quad \langle T\rangle^f=\langle T\rangle^s=T_w\quad \text{for } y=0 \tag{16}$$

$$\langle v\rangle^f=-v_0,\quad \langle T\rangle^f=T_{in},\quad \frac{\partial\langle T\rangle^s}{\partial y}=0\quad \text{for } y=H \tag{17}$$

Eqs. (8)–(10) can be further simplified. For this, it is assumed that the aspect ratio of the channel is much higher than 1 and the solid conductivity is higher than the fluid conductivity.

$$H,L\gg w_c,\quad k_s\gg k_f \tag{18}$$

Estimating the order of magnitude of each term appearing on the right-hand side of Eqs. (8) and (9), we have

$$\mu_f\frac{U_f}{w_c^2}\gg\mu_f\frac{U_f}{L^2},\mu_f\frac{U_f}{H^2} \tag{19}$$

$$\mu_f\frac{V_f}{w_c^2}\gg\mu_f\frac{V_f}{L^2},\mu_f\frac{V_f}{H^2} \tag{20}$$

Combining Eqs. (10) and (11), we have

$$\varepsilon\rho_f c_f\left(\langle u\rangle^f\frac{\partial\langle T\rangle^{b,f}}{\partial x}+\langle v\rangle^f\frac{\partial\langle T\rangle^{b,f}}{\partial y}\right)=(1-\varepsilon)k_s\frac{\partial\langle T\rangle^s}{\partial x^2}+\varepsilon k_f\frac{\partial\langle T\rangle^{b,f}}{\partial x^2}+(1-\varepsilon)k_s\frac{\partial\langle T\rangle^s}{\partial y^2}+\varepsilon k_f\frac{\partial\langle T\rangle^{b,f}}{\partial y^2} \tag{21}$$

Estimating the order of magnitude of each term appearing on the right-hand side of Eq. (21), it follows that

$$\frac{k_sT}{L^2}\gg\frac{k_fT}{L^2},\quad \frac{k_sT}{H^2}\gg\frac{k_fT}{H^2} \tag{22}$$

From the relations shown in Eqs. (19), (20), and (22), the simplified forms of Eqs. (8)–(10) are given as

$$\frac{6}{5}\rho_f\left(\langle u\rangle^f\frac{\partial\langle u\rangle^f}{\partial x}+\langle v\rangle^f\frac{\partial\langle u\rangle^f}{\partial y}\right)+\frac{\partial\langle p\rangle^f}{\partial x}=-\frac{\varepsilon\mu_f}{K}\langle u\rangle^f \tag{23}$$

$$\frac{6}{5}\rho_f\left(\langle u\rangle^f\frac{\partial\langle v\rangle^f}{\partial x}+\langle v\rangle^f\frac{\partial\langle v\rangle^f}{\partial y}\right)+\frac{\partial\langle p\rangle^f}{\partial y}=-\frac{\varepsilon\mu}{K}\langle v\rangle^f \tag{24}$$

$$\varepsilon\rho_f c_f\left(\langle u\rangle^f\frac{\partial\langle T\rangle^{b,f}}{\partial x}+\langle v\rangle^f\frac{\partial\langle T\rangle^{b,f}}{\partial y}\right)=ha(\langle T\rangle^s-\langle T\rangle^{b,f}) \tag{25}$$

Partial differential governing equations (Eqs. (11) and (23)–(25)) can be transformed into an ordinary differential equation with a similarity variable. The similarity variable η, the stream function Ψ, and the dimensionless temperatures are defined as

$$\eta=y\sqrt{\frac{v_0\rho_f}{H\mu_f}} \tag{26}$$

$$\Psi=\sqrt{\frac{v_0\mu_f}{H\rho_f}}F(\eta)x \tag{27}$$

$$\theta^{b,f}(\eta)=\frac{\langle T\rangle^{b,f}-T_w}{T_{in}-T_w} \tag{28}$$

$$\theta^s(\eta)=\frac{\langle T\rangle^s-T_w}{T_{in}-T_w} \tag{29}$$

With Eqs. (26)–(29), the governing equations (Eqs. (11) and (23)–(25)) and the boundary conditions (Eqs. (16) and (17)) are given as

$$\frac{6}{5}FF''+\frac{6}{5}(1-F'F')+\frac{\varepsilon}{K}\frac{H\mu_f}{v_0\rho_f}(1-F')=0 \tag{30}$$

$$-\varepsilon\rho_f c_f\left(\frac{v_0}{H}\right)F\theta^{b,f\prime}=ha(\theta^s-\theta^{b,f}) \tag{31}$$

$$(1-\varepsilon)k_s\left(\frac{v_0\rho_f}{H\mu_f}\right)\theta^{s\prime\prime}+ha(\theta^{b,f}-\theta^s)=0 \tag{32}$$

$$F=0,\quad \theta^s=0\quad \text{for } \eta=0 \tag{33}$$

$$F'=1,\quad \theta^{b,f}=1,\quad \theta^{s\prime}=0\quad \text{for } \eta=\sqrt{\frac{v_0H\rho_f}{\mu_f}} \tag{34}$$

By solving Eq. (30), the following equations for the velocity distribution are obtained.

$$F=\eta \tag{35}$$

$$u=\frac{\partial\Psi}{\partial y}=\frac{v_0}{H}x,\quad v=-\frac{\partial\Psi}{\partial x}=-\frac{v_0}{H}y \tag{36}$$

In general, Eqs. (31) and (32) cannot be solved analytically. However, when we assume the fin efficiency is 1, the following equations for the temperature distribution can be obtained.

$$\theta^s=0,\quad \theta^{b,f}=\left(\frac{\eta}{\sqrt{v_0H\rho_f/\mu_f}}\right)^{\frac{ha}{\varepsilon\rho_f c_f}\left(\frac{H}{v_0}\right)} \tag{37}$$

$$\langle T\rangle^s=T_w,\quad \langle T\rangle^{b,f}=(T_{in}-T_w)\left(\frac{y}{H}\right)^{\frac{ha}{\varepsilon\rho_f c_f}\left(\frac{H}{v_0}\right)}+T_w \tag{38}$$

Finally, the pressure drop between the inlet and the outlet of the heat sink and the thermal resistance are obtained, respectively, from Eqs. (36) and (38).

$$\Delta p_{plate}=\frac{1}{L}\int_{-L/2}^{L/2}\langle p\rangle^f_{y=H}dx-\frac{1}{H}\int_0^H\langle p\rangle^f_{x=L/2}dy=\rho v_0^2\left(\frac{1}{10}\frac{L^2}{H^2}-\frac{2}{5}\right)+\frac{\varepsilon\mu_f H}{K}v_0\left(\frac{1}{12}\frac{L^2}{H^2}+\frac{1}{3}\right) \tag{39}$$

$$R_{plate}=\frac{T_w-T_{in}}{q}=\left(\varepsilon\rho_f c_f v_0L^2\left(1-\left(1+\frac{haH}{\varepsilon\rho_f c_f v_0}\right)^{-1}\right)\right)^{-1} \tag{40}$$

When the fin efficiency is not 1, the approximate value of the thermal resistance is given from Eq. (40) by using the fin model as follows:

$$R_{plate}=\left(\varepsilon\rho_f c_f v_0L^2\left(1-\left(1+\frac{\eta_{eff}haH}{\varepsilon\rho_f c_f v_0}\right)^{-1}\right)\right)^{-1} \tag{41}$$

where η_{eff} is the fin efficiency.

$$\eta_{eff} = \frac{\tanh\left(H\sqrt{\frac{ha}{k_s(1-\varepsilon)}}\right)}{H\sqrt{\frac{ha}{k_s(1-\varepsilon)}}} \tag{42}$$

When $\frac{\eta_{eff}haH}{\varepsilon\rho_f c_f v_0} \gg 1$, Eq. (41) becomes

$$R_{plate} = (\varepsilon\rho_f c_f v_0 L^2)^{-1} \tag{43a}$$

On the other hand, when $\frac{\eta_{eff}haH}{\varepsilon\rho_f c_f v_0} \ll 1$, Eq. (41) becomes

$$R_{plate} = (\eta_{eff}haHL^2)^{-1} \tag{43b}$$

Eqs. (43a) and (43b) correspond to low and high pumping-power conditions, respectively.

Eqs. (39) and (41) are derived without adopting correlations for the friction factor and the Nusselt number for a parallel flow. Instead, it is assumed that the velocity and temperature profiles for the fluid in the averaging direction are similar to those of a Poiseuille flow between two infinite parallel plates, as shown in Eqs. (6) and (7). This assumption is reasonable but is not exact, because the velocity and temperature profiles for an impinging flow are not exactly the same as those for the flow between two infinite parallel plates. Therefore, the permeability K and the heat transfer coefficient h presented in Eqs. (14) and (15) should be modified in order to better predict the pressure drop and the thermal resistance. In the present study, the appropriate values for K and h are determined from the experimental data for the pressure drop and the thermal resistance with Eqs. (39) and (41), respectively. Finally, the modified parameters obtained from experimental investigations are given as follows.

$$K = \frac{\varepsilon w_c^2}{12((0.289 + 16.0w_c^*) + (0.00263 + 0.133w_c^*)\mathrm{Re}_{w_c})} \tag{44}$$

$$h = \frac{70k_f}{17w_c}((17.4w_c^* - 63.4(w_c^*)^2) + (7.67\times10^{-3})w_c^*\mathrm{Re}_{w_c}) \tag{45}$$

3.2. Pin-fin heat sink

The fluid flow in the pin-fin heat sink is axisymmetric in nature rather than two-dimensional. In the present study, the pin-fin heat sink is modeled as an equivalent porous cylinder which has the same porosity, wetted surface, and base area. The top view for the equivalent porous cylinder is shown in Fig. 2(b). By solving Eqs. (11) and (23)–(25) in cylindrical coordinates, the pressure drop between the inlet and the outlet of the heat sink and the thermal resistance are given, respectively, as

$$\Delta p_{pin} = \rho v_0^2\left(\frac{3}{40}\frac{R_0^2}{H^2} - \frac{2}{5}\right) + \frac{\varepsilon\mu_f H}{K}v_0\left(\frac{1}{8}\frac{R_0^2}{H^2} + \frac{1}{3}\right) \tag{46}$$

$$R_{pin} = \left(\varepsilon\rho_f c_f v_0\pi R_0^2\left(1 - \left(1 + \frac{\eta_{eff}haH}{\varepsilon\rho_f c_f v_0}\right)^{-1}\right)\right)^{-1} \tag{47}$$

where

$$\varepsilon = 1 - \left(\frac{w_w}{w_w + w_c}\right)^2, \quad a = \frac{4w_w}{(w_w + w_c)^2}, \quad R_0 = \sqrt{L^2/\pi} \tag{48}$$

$$K = \frac{\varepsilon w_c^2}{12((0.232 + 10.4w_c^*) + (0.000376 + 0.0840w_c^*)\mathrm{Re}_{w_c})} \tag{49}$$

$$h = \frac{70k_f}{17w_c}((9.96w_c^* - 28.3(w_c^*)^2) + (6.41\times10^{-4})\mathrm{Re}_{w_c}) \tag{50}$$

When $\frac{\eta_{eff}haH}{\varepsilon\rho_f c_f v_0} \gg 1$, Eq. (47) becomes

$$R_{pin} = (\varepsilon\rho_f c_f v_0\pi R_0^2)^{-1} \tag{51a}$$

On the other hand, when $\frac{\eta_{eff}haH}{\varepsilon\rho_f c_f v_0} \ll 1$, Eq. (47) becomes

$$R_{pin} = \frac{T_w - T_{in}}{q} = (\eta_{eff}haH\pi R_0^2)^{-1} \tag{51b}$$

Eqs. (51a) and (51b) correspond to low and high pumping-power conditions, respectively.

The value of the present model lies in its simplicity. The pressure drop and thermal resistance for the plate-fin heat sink are easily obtained by solving Eqs. (39) and (41), respectively, together with Eqs. (44) and (45). On the contrary, the model suggested by Kondo et al. [6] consists of dozens of equations and requires tedious calculation process. However, the applicability of the suggested model is limited because the permeability K and the heat transfer coefficient h are obtained from experimental data. The present model is applicable for

$$5\times10^9 \le P_{Pump}^* \le 10^{11}, \quad 1 \le L^* \le 2 \tag{52}$$

for which the experiment is conducted.

4. Results and discussion

The pressure drop and the thermal resistance obtained from experiments are compared with those from the proposed model. As shown in Fig. 6, the experimental results of the pressure drop

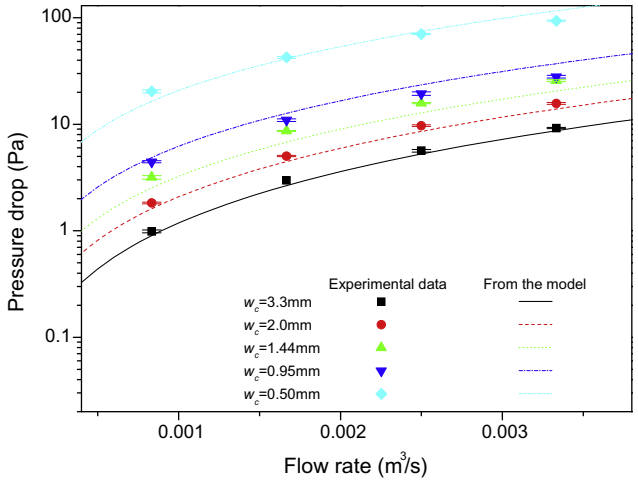

(a) Plate-fin heat sinks

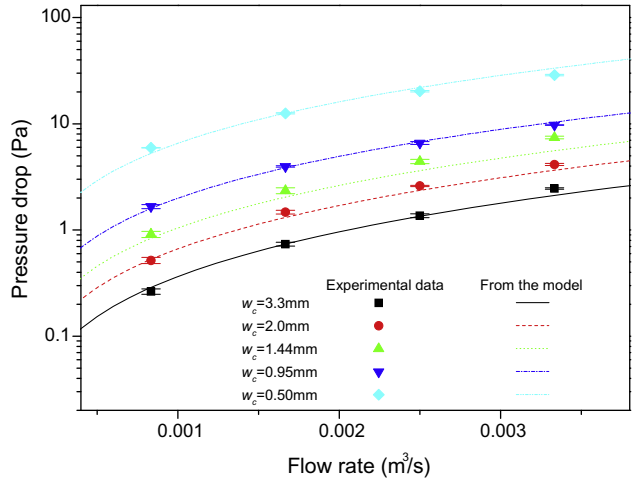

(b) Pin-fin heat sinks

Fig. 6. Pressure drop (L = 40 mm, H = 25 mm, w_w = 1 mm).

are in close agreement with the predictions from the present model within a maximum error of 31% for the plate-fin heat sinks and 22% for the pin-fin heat sinks, respectively. As shown in Fig. 7, results for the thermal resistance obtained from the experiments and the model match well within a maximum error of 20% for the plate-fin heat sinks and 13% for the pin-fin heat sinks, respectively. The close agreement between experiment and prediction is because the permeability and heat transfer coefficient are determined from the experimental side of the work. From Figs. 6 and 7, it is concluded that Eqs. (44), (45), (49), and (50) are reasonable choices for the permeability and the heat transfer coefficient.

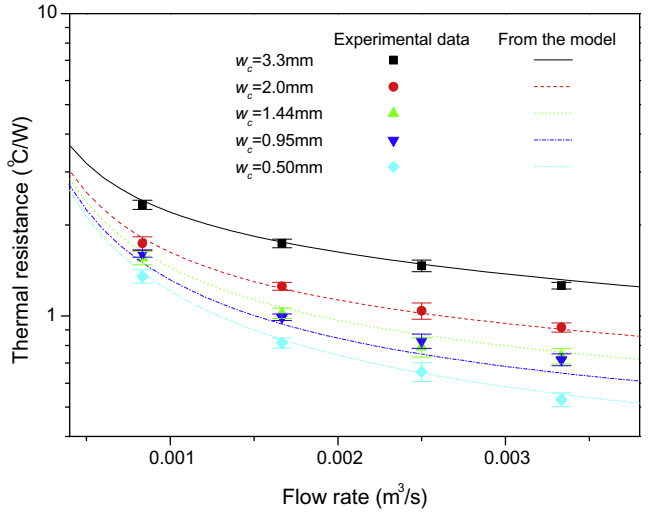

(a) Plate-fin heat sinks

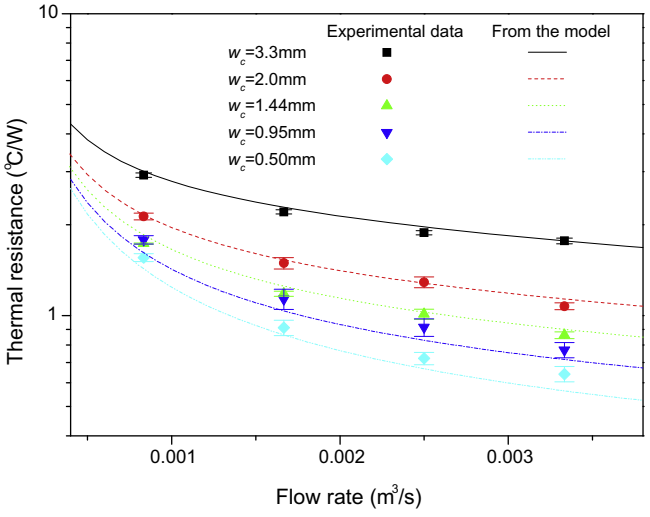

(b) Pin-fin heat sinks

Fig. 7. Thermal resistance (L = 40 mm, H = 25 mm, w_w = 1 mm).

Using the models for the plate-fin and pin-fin heat sinks, their thermal resistances are calculated. Then, we numerically optimize the dimensions for the plate-fin and pin-fin heat sinks by using the gradient descent algorithm. The optimized structures for which the thermal resistances are minimized under the fixed pumping power are then obtained, as listed in Table 2. The constraint for the fixed pumping power physically means that the power required to drive the coolant through the heat sinks is fixed. Finally, by comparing the thermal resistances of the optimized plate-fin and pin-fin heat sinks, a contour map for an impinging flow configuration is presented in Fig. 8. Fig. 8 depicts the ratio of the thermal resistances of the optimized plate-fin and pin-fin heat sinks $R_{opt,plate}/R_{opt,pin}$ as a function of dimensionless pumping power and dimensionless length. This ratio was successfully used for comparing thermal performances of plate-fin and pin-fin heat sinks with parallel-flow configuration [18]. In Fig. 8, in the region where the ratio is above 1, the thermal resistance of the optimized pin-fin heat sink is smaller than that of the optimized plate-fin heat sink. On the other hand, the thermal resistance of the optimized plate-fin heat sink is smaller than that of the optimized plate-fin heat sink when the ratio is below 1.

The contour map for an impinging flow configuration indicates the following: Optimized pin-fin heat sinks have lower thermal resistances than optimized plate-fin heat sinks only when the dimensionless pumping power is small and the dimensionless length of heat sinks is large. In other words, the pin-fin heat sink shows better performance than the plate-fin heat sink as the pumping power per unit of heat sink volume decreases. It is worth mentioning that Fig. 8, which describes the comparison of the thermal performance of the optimized plate-fin and pin-fin heat sinks, is helpful in determining the best designs for heat sinks.

For the plate-fin heat sink, impinging air flows out only along the y-axis. On the contrary, air can flow out in every direction for the pin-fin heat sink. Hence, the flow impedance of the optimized pin-fin heat sink is typically lower than that of the optimized plate-fin heat sink, and the inlet velocity of the optimized pin-fin heat sink is higher than that of the optimized plate-fin heat sink under the fixed pumping-power condition, as shown in Fig. 9. From Eqs. (43a) and (51a), it can be shown that $R_{opt,plate}/R_{opt,pin}$ is proportional

Table 2
Comparison of geometries and thermal resistances for optimized heat sinks.

Dimensionless pumping power $\frac{P_{pump}}{\mu^3\rho^{-2}H^{-1}}$	Dimensionless length $\frac{L}{H}$	Type of heat sink	Optimum channel width (mm) $w_{c,opt}$	Optimum fin thickness (mm) $w_{w,opt}$	Optimum thermal resistance (K/W) R_{opt}
3×10^{10}	1	Plate-fin	0.763	0.202	1.76
		Pin-fin	0.716	0.807	1.93
6×10^{10}	1	Plate-fin	0.639	0.185	1.48
		Pin-fin	0.578	0.677	1.65
9×10^{10}	1	Plate-fin	0.576	0.175	1.34
		Pin-fin	0.511	0.614	1.50
3×10^{10}	2	Plate-fin	1.15	0.233	0.747
		Pin-fin	1.09	1.10	0.734
6×10^{10}	2	Plate-fin	0.977	0.217	0.617
		Pin-fin	0.881	0.917	0.620
9×10^{10}	2	Plate-fin	0.884	0.207	0.553
		Pin-fin	0.779	0.830	0.562

H = 25 mm, ρ_f = 1.1774 kg/m^3, μ_f = 1.8462 × 10^{-5} kg/m s, c_f = 1.0057 × 10^3 J/kg K, k_f = 0.02624 W/m K, k_s = 171 W/m K.

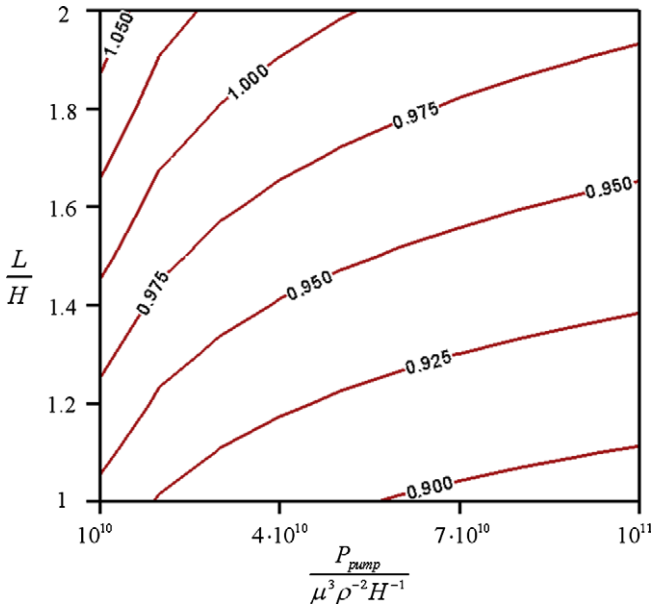

Fig. 8. Ratios of the thermal resistances of the optimized plate-fin and pin-fin heat sinks ($k_s/k_f = 6.4 \times 10^3$, $Pr = 0.707$).

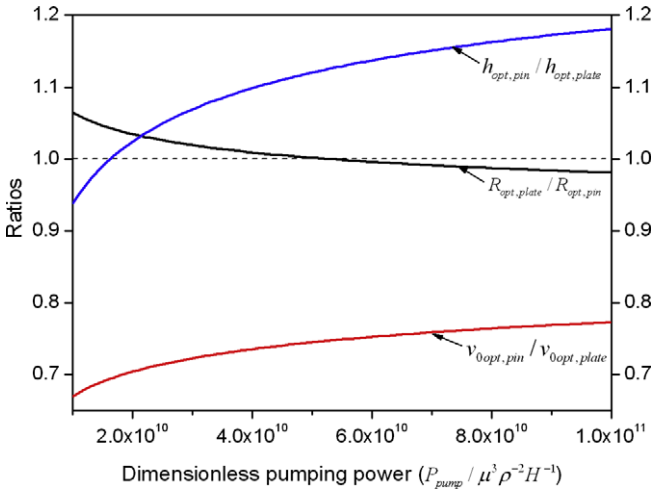

Fig. 9. Ratios of the thermal resistances, inlet velocities, and heat transfer coefficients of the optimized plate-fin and pin-fin heat sinks ($k_s/k_f = 6.4 \times 10^3$, $Pr = 0.707$, $L/H = 2$).

to $v_{0opt,pin}/v_{0opt,plate}$ when the pumping power per unit of heat sink volume is small. Therefore, the pin-fin heat sink shows better performance than the plate-fin heat sink when the pumping power per unit of heat sink volume is small. On the other hand, Eqs. (43b) and (51b), it can be shown that $R_{opt,plate}/R_{opt,pin}$ is proportional to $h_{opt,pin}/h_{opt,plate}$ when the pumping power per unit of heat sink volume is large. As shown in Fig. 9, the optimized plate-fin heat sink has a higher heat transfer coefficient than the optimized pin-fin heat sink for high dimensionless pumping powers. Therefore, the plate-fin heat sink shows better performance than the pin-fin heat sink when the pumping power per unit of heat sink volume is large.

5. Conclusion

In this paper, we compared thermal performances of plate-fin and pin-fin heat sinks subject to an impinging flow. Experimental investigations were performed for various flow rates and channel widths. From experimental data, we suggested a model based on the volume averaging method for predicting the pressure drop and the thermal resistance. Using the proposed model, thermal resistances of the optimized plate-fin and pin-fin heat sinks were compared under fixed pumping-power conditions. It was shown that optimized pin-fin heat sinks possess lower thermal resistances than optimized plate-fin heat sinks when dimensionless pumping power is small and the dimensionless length of heat sinks is large. On the contrary, the optimized plate-fin heat sinks have smaller thermal resistances when dimensionless pumping power is large and the dimensionless length of heat sinks is small.

Acknowledgements

This work was supported by the Korea Science and Engineering Foundation (KOSEF) through the National Research Lab. Program funded by the Ministry of Science and Technology (No. M10600000224O6J000022410).

References

[1] S. Oktay, R.J. Hannemann, A. Bar-Cohen, High heat from a small package, Mech. Eng. 108 (3) (1986) 36–42.
[2] A. Bar-Cohen, Thermal management of electric components with dielectric liquids, in: J.R. Lloyd, Y. Kurosaki (Eds.), Proceedings of ASME/JSME Thermal Engineering Joint Conference, vol. 2, 1996, pp. 15–39.
[3] F.P. Incropera, Convection heat transfer in electronic equipment cooling, J. Heat Transfer 110 (1988) 1097–1111.
[4] W. Nakayama, Thermal management of electronic equipment: a review of technology and research topics, Appl. Mech. Rev. 39 (12) (1986) 1847–1868.
[5] C.R. Biber, Pressure drop and heat transfer in an isothermal channel with impinging flow, IEEE Trans. Components Pack. Manuf. Technol. A 20 (1997) 458–462.
[6] Y. Kondo, M. Behnia, W. Nakayama, H. Matsushima, Optimization of finned heat sinks for impingement cooling of electronic packages, J. Electronic Pack. (1998) 259–266.
[7] Z. Duan, Y.S. Muzychka, Experimental investigation of heat transfer in impingement air cooled plate fin heat sinks, J. Electronic Pack. 128 (2006) 412–418.
[8] S. Sathe, K.M. Kelkar, K.C. Karki, C. Tai, C. Lamb, S.V. Patankar, Numerical prediction of flow and heat transfer in an impingement heat sink, J. Electronic Pack. 119 (1997) 58–63.
[9] G. Ledezma, A.M. Morega, A. Bejan, Optimal spacing between pin fins with impinging flow, J. Heat Transfer 118 (1996) 570–577.
[10] Y. Kondo, H. Matsushima, T. Komatsu, Optimization of pin fin heat sinks for impingement cooling of electronic packages, J. Electronic Pack. 122 (2000) 240–246.
[11] J.S. Issa, A. Ortega, Experimental measurements of the flow and heat transfer of a square jet impinging on an array of square pin fins, J. Electronic Pack. 128 (2006) 61–70.
[12] Y. Kondo, H. Matsushima, S. Ohashi, Optimization of heat sink geometries for impingement air-cooling of LSI packages, Heat Transfer Asian Res. 28 (1999) 138–151.
[13] H.-Y. Li, S.-M. Chao, G.-L. Tsai, Thermal performance measurement of heat sinks with confined jet by infrared thermography, Int. J. Heat Mass Transfer 48 (2005) 5386–5394.
[14] S.J. Kim, J.W. Yoo, S.P. Jang, Thermal optimization of a circular-sectored finned tube using a porous medium approach, J. Heat Transfer 124 (2002) 1026–1033.
[15] D.-K. Kim, S.J. Kim, Averaging approach for microchannel heat sinks subject to the uniform wall temperature condition, Int. J. Heat Mass Transfer 49 (2006) 695–706.
[16] V.C. Slattery, Advanced Transport Phenomena, Cambridge University Press, Cambridge, 1999.
[17] A. Bejan, Convective Heat Transfer, third ed., John Wiley & Sons, Inc., New York, 2004. pp. 42–49.
[18] S.J. Kim, D.-K. Kim, H.H. Oh, Comparison of fluid flow and thermal characteristics of plate-fin and pin-fin heat sinks subject to a parallel flow, Heat Transfer Eng. 29 (2008) 169–177.